

# Chapter 2

## Reconstruction of Solar Subsurfaces by Local Helioseismology

Alexander G. Kosovichev and Junwei Zhao

**Abstract** Local helioseismology has opened new frontiers in our quest for understanding of the internal dynamics and dynamo on the Sun. Local helioseismology reconstructs subsurface structures and flows by extracting coherent signals of acoustic waves traveling through the interior and carrying information about subsurface perturbations and flows, from stochastic oscillations observed on the surface. The initial analysis of the subsurface flow maps reconstructed from the 5 years of SDO/HMI data by time-distance helioseismology reveals the great potential for studying and understanding of the dynamics of the quiet Sun and active regions, and the evolution with the solar cycle. In particular, our results show that the emergence and evolution of active regions are accompanied by multi-scale flow patterns, and that the meridional flows display the North-South asymmetry closely correlating with the magnetic activity. The latitudinal variations of the meridional circulation speed, which are probably related to the large-scale converging flows, are mostly confined in shallow subsurface layers. Therefore, these variations do not necessarily affect the magnetic flux transport. The North-South asymmetry is also pronounced in the variations of the differential rotation ('torsional oscillations'). The calculations of a proxy of the subsurface kinetic helicity density show that the helicity does not vary during the solar cycle, and that supergranulation is a likely source of the near-surface helicity.

### 2.1 Introduction

Observations of solar oscillations provide a unique opportunity to obtain information about the structure and dynamics of the solar interior beneath the visible surface. The oscillations with a characteristic period of 5 min represent acoustic waves stochastically excited by the turbulent convection in a shallow subsurface layer. The excitation mechanism has not been completely understood. However,

---

A.G. Kosovichev (✉) • J. Zhao  
New Jersey Institute of Technology, Newark, NJ 07103, USA  
Stanford University, Stanford, CA 95305, USA  
e-mail: sasha@bbso.njit.edu

recent numerical simulations have shown that the waves can be excited due to the interaction of turbulent vortex tubes ubiquitously generated in the intergranular lanes (Kitiashvili et al. 2011). These stochastic waves produce chaotic oscillation patterns on the solar surface. However, a spectral analysis of the time series of these patterns reveals that most of the oscillation power is concentrated in a set of normal modes (Fig. 2.1a). These modes represent standing acoustic waves trapped in the subsurface layers by their reflection between the sharp density gradient near the surface, and the increasing sound speed in the interior. The depth of the inner reflection depends on the horizontal wavelength of the oscillations. The horizontal wavelength,  $\lambda_h$ , is usually represented in terms of the spherical harmonic degree,  $\ell = 2\pi R/\lambda_h$ . The oscillation frequency is expressed in terms of cyclic frequency  $\nu = \omega/2\pi$ . In the  $\ell - \nu$  diagram shown in Fig. 2.1a, the lowest ridge represents the surface gravity mode ( $f$ -mode). The other ridges are acoustic modes of various radial order  $n$ , which is equal to the number of nodes along the radius. This number is higher for higher frequency ridges. The time-series of solar oscillations have been obtained almost uninterruptedly since 1995 from the ground-based network GONG and space mission SOHO (Solar and Heliospheric Observatory) and SDO (Solar Dynamics Observatory). The oscillation frequencies are routinely measured from 72- and 108-day time series by fitting the modal lines which are used for

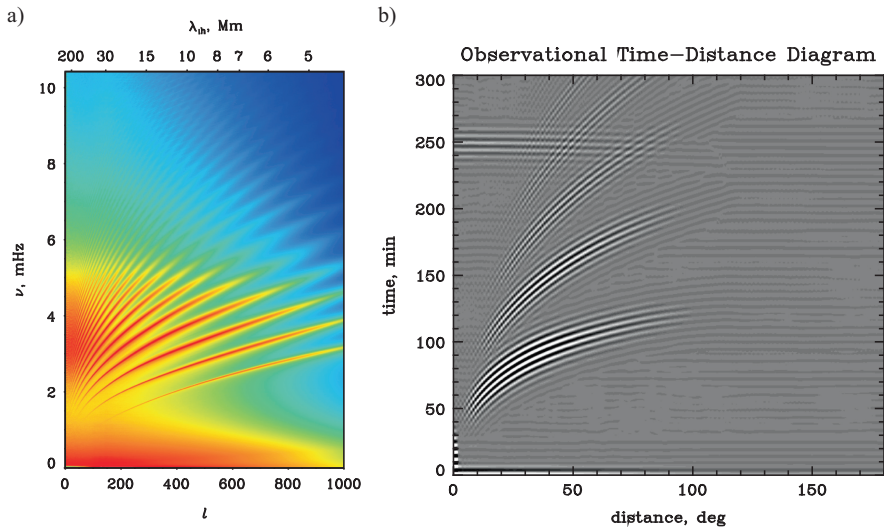


**Fig. 2.1** (a) The power spectrum of solar oscillations as a function of the angular degree  $\ell$ , and cyclic frequency,  $\nu$ . The enhanced power corresponds to the normal oscillation modes of the Sun. (b) The cross-covariance function ('time-distance diagram') of solar oscillations as a function of the distance between the correlation points on the solar surface and the time lag of the cross-covariance. The lowest ridge is formed by acoustic wave packets traveling between two surface points ('source' and 'receiver') through the solar interior (so-called, the first skip); the higher ridges are formed by the wave packets arriving to the receiver after additional reflections from the surface (the 'second' skip, and so on)

inferring variations of the sound speed, asphericity, and differential rotation rate. This approach called ‘global helioseismology’ has provided important information about the structure, composition and dynamics of the solar interior. In particular, it was led to the discovery of a sharp radial gradient of the differential rotation at the base of the convection zone (Kosovichev 1996b), the so-called tachocline, the near-surface rotational shear layer (Schou et al. 1998), subsurface zonal flows migrating with the solar activity cycle (Kosovichev and Schou 1997). Recent analysis of the high-degree oscillation modes revealed a sharp gradient of the sound speed in a narrow 30 Mm deep layer just beneath the solar surface (Reiter et al. 2015). This layer (called ‘leptocline’, Godier and Rozelot 2001) presumably plays an important role in the solar dynamo (Pipin and Kosovichev 2011).

It is important to note that while the oscillation power spectrum extends into the high-frequency region (10 mHz and higher), only the ridge parts with the frequency below the acoustic cut-off frequency (which is approximately at 5.2 mHz) represent the normal modes. The higher frequency parts correspond to so-called ‘pseudo-modes’. The pseudo-modes are formed by interference between the waves traveling from the excitation sources directly to the surface and the waves which come to the same surface location after reflection in the interior. The pseudo-mode ridges are close to the mode ridges (so that the ridges look continuous) because the excitation sources are located very close to the surface where the oscillations are observed. The pseudo-mode frequencies depend on details of the excitation mechanism and on the wave interaction with the solar atmosphere. Therefore, so-far, only the normal modes have been used for the reconstruction of solar subsurfaces. The primary restriction of global helioseismology is that it can only reconstruct the azimuthally averaged properties of the interior. This is not sufficient for the understanding of the solar dynamics and magnetism.

The three-dimensional structure of the solar subsurfaces can be reconstructed by techniques of local helioseismology. One of these techniques, called ‘ring-diagram analysis’ (Gough and Toomre 1983) is based on measuring frequency shifts in local (typically  $15 \times 15$  deg) areas, and uses the global helioseismology description of the mode frequency sensitivity to local sound-speed variations and flows. This technique allows us to reconstruct the solar subsurfaces with relatively low spatial resolution in shallow regions. The reconstruction with higher spatial resolution and much deeper in the interior can be achieved by methods based on extracting coherent wave signals and measuring variations of the wave travel times or phase shift. These techniques called time-distance helioseismology (Duvall et al. 1993) and acoustic holography (Lindsey and Braun 2000) employ cross-covariance functions of solar oscillations instead of the power spectral analysis. The discovery that coherent signals, such as wave packets, can be extracted from the cross-covariance functions of the stochastic solar oscillations (Fig. 2.1b) was made by Duvall et al. (1993). This approach was then developed in helioseismology, terrestrial seismology, and other disciplines, and in broader applications is called ‘ambient noise imaging’. The foundation of this approach is based on the property of cross-covariance functions to represent wave signals corresponding to point sources. Roughly speaking the cross-covariance function can be considered as the Green’s function of the solar

wave equation. In real solar conditions this is only an approximation because of the limited frequency bandwidth of solar oscillations and inhomogeneities of the solar structures and distribution of the stochastic sources. A complete theory of this approach of helioseismology has not been developed. It requires extensive studies of wave interaction with turbulence, flows and magnetic field. Nevertheless, the initial results based on relatively simple descriptions of wave propagation have provided important insights into the three-dimensional structures and flow patterns of the solar subsurfaces. The primary focus of these studies is mapping the flow patterns associated with the solar cycle, and formation and evolution of active regions.

In the current state of local helioseismology the systematic errors as well as effects of the stochastic realization noise have not been fully investigated. These studies require substantial effort for modeling the wave dynamics in realistic solar conditions, and require 3D MHD simulations on large supercomputer systems. The validation and testing of the time-distance technique have been performed by comparing the helioseismic inversions in the shallowest layer with the surface flows obtained by a local correlation tracking technique (Liu et al. 2013), and through the analysis and inversion of numerical simulation data for subsurface flows and sound-speed variations (Birch et al. 2011; Hartlep et al. 2013; Parchevsky and Kosovichev 2009; Parchevsky et al. 2014). The testing for regions with strong magnetic field has not yet been completed. However, the simulations of the wave propagation in sunspot models showed that one of the primary effects in sunspot regions is the wave reflection from deeper layers, compared to the quiet-Sun regions, where the plasma parameter,  $\beta = 8\pi P/B^2$ , the ratio of the gas pressure to magnetic pressure, is equal to unity (this layer also corresponds to the deeper photospheric surface of sunspots, known as the Wilson depression). Below the Wilson depression level the gas pressure dominates, and the helioseismic acoustic waves behave like fast MHD waves: the wave speed becomes anisotropic, and also depends on the temperature stratification beneath sunspots. The magnetic and temperature effects have not been separated in the wave-speed inversion results (Kosovichev et al. 2000). This is an important task of local helioseismology. One of the difficulties is that the limited computer power has not allowed to simulated the sunspot models sufficiently large and deep for the helioseismology testing, so that the wave properties are not affected by the boundary conditions of the simulations. A comparison of the wave-speed inversions obtained for a sunspot regions by the time-distance and ring-diagram techniques (see Kosovichev 2012; Kosovichev et al. 2011 and references therein) shows a good qualitative agreement: both inversions show a two-layer structure with a layer of reduced wave speed beneath the surface followed by a layer of an increased wave speed. However, the depth of these layers is different, perhaps, because of the drastically different spatial resolution, and different contributions of magnetic field. A comparison of the time-distance and acoustic holography inversion results has been performed by using artificial simulation data (Birch et al. 2011; Parchevsky et al. 2014).

## 2.2 Time-Distance Helioseismology from SDO

This brief review presents recent results obtained by the helioseismology reconstructions of subsurface flows in the near-surface layer and development of active regions. The results are obtained by analyzing inversions for subsurface flows from the SDO Joint Science Operations Center (JSOC) at Stanford University (Scherrer et al. 2012). The JSOC data analysis pipeline provides 3D maps of solar flows covering almost the whole disk (within 60 deg from the disk center) in the range of depths from 0 to 30 Mm, every 8 h.

The time-distance helioseismology pipeline (Fig. 2.2a) developed by the Stanford group (Couvidat et al. 2012; Zhao et al. 2012) utilizes two different methods for

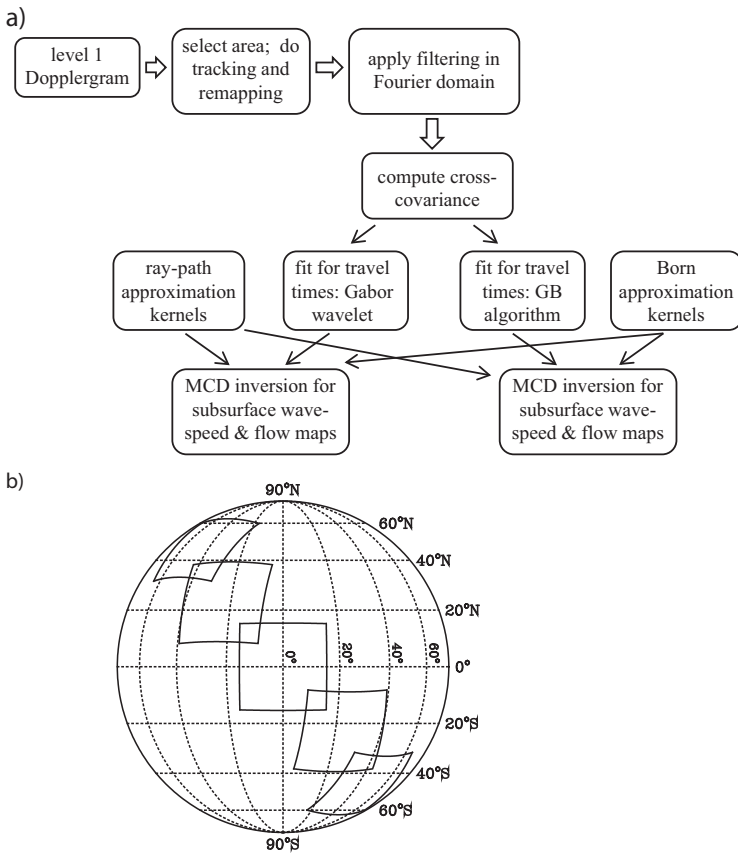


**Fig. 2.2** (a) A scheme of the Time-Distance Helioseismology Pipeline implemented at the Joint Science Operations Center (JSOC) for Solar Dynamics Observatory at Stanford University (Zhao et al. 2012); (b) Illustration of the surface locations of the individual patches used for inferences of the subsurface structure and flows; the total 25 patches are used to cover  $120 \times 120$  deg of the disk area

measuring the acoustic travel times: (1) the method of fitting the Gabor wavelet to the cross-covariance function, which provides measurements of both the phase and group travel times (Kosovichev and Duvall 1997) and (2) the method of calculating the travel-time shift relative to a reference cross-covariance function (Gizon and Birch 2002), usually calculated for a quiet-Sun region. The two sets of the travel times are calculated independently for 11 travel distances, for the same 25 areas covering the solar disk (Fig. 2.2b), and for the same 8-h intervals. Then, the travel times are used for reconstruction of subsurface flows in 11 subsurface layers in the depth ranges: 1–3, 3–5, 5–7, 7–10, 10–13, 13–17, 17–21, 21–26, 26–30, and 30–35 Mm, and with the horizontal spatial sampling of 0.12 deg (1.5 Mm).

The inversions are performed by using two different methods for calculating the travel-time sensitivity functions: (1) the ray-path approximation (Kosovichev 1996a; Kosovichev and Duvall 1997) and (2) the first Born approximation (Birch and Kosovichev 2000, 2001; Birch et al. 2001, 2004; Birch and Gizon 2007). The inversions are performed using the Multi-Channel Deconvolution (MCD) technique (Jacobsen et al. 1999) for the two independent travel-time measurements using the two types of the sensitivity kernels. Therefore, the pipeline output consists of four sets of subsurface flow maps for the same areas on the Sun (Zhao et al. 2012). This allows the comparison of the different approaches and estimate potential systematic errors. The reconstruction of subsurface flows has also been tested through analysis and inversion of numerical simulation results as well as by the comparison of the flow maps obtained by the different techniques, and also by comparing the inversion results in the shallowest layer with the surface flows measured by the feature correlation tracking techniques (Liu et al. 2013). Figure 2.3 illustrates the comparison of the flow maps below a sunspot region, obtained by using two different techniques for measuring the travel times and two different models for the travel-time sensitivity functions. The results show that the agreement is quite good everywhere except the areas close to the sunspot. As discussed in the Introduction, the effects of a strong magnetic field and large perturbations of the thermodynamic structure have not been fully investigated. Solving this problem requires more studies of systematic uncertainties using realistic numerical simulations. Nevertheless, the currently available inferences shed light on the intriguing dynamics of the solar interior.

## 2.3 Subsurface Flows and Effects of Solar Activity

An example of the reconstructed subsurface flow maps is illustrated in Fig. 2.4a, which shows the distribution of the divergence of the horizontal flow velocity in the depth range 1–3 Mm. The primary feature covering the whole surface is supergranulation. The outflows of a few hundred m/s in the supergranulation cells are represented by light dot-like features. However, the examination of these maps shows that in the vicinity of magnetic active regions (shown in Fig. 2.4b), the supergranulation pattern is substantially suppressed. The flow pattern beneath and

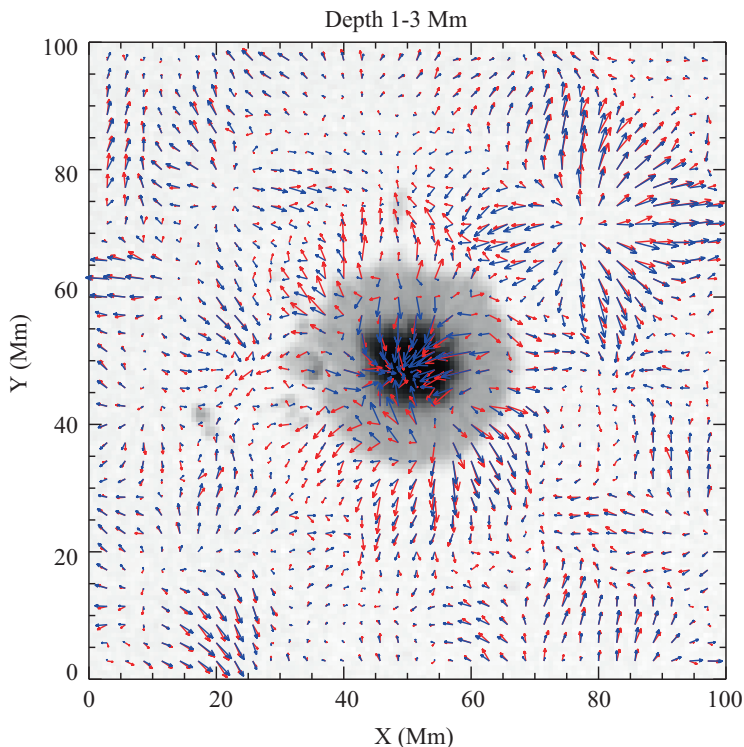


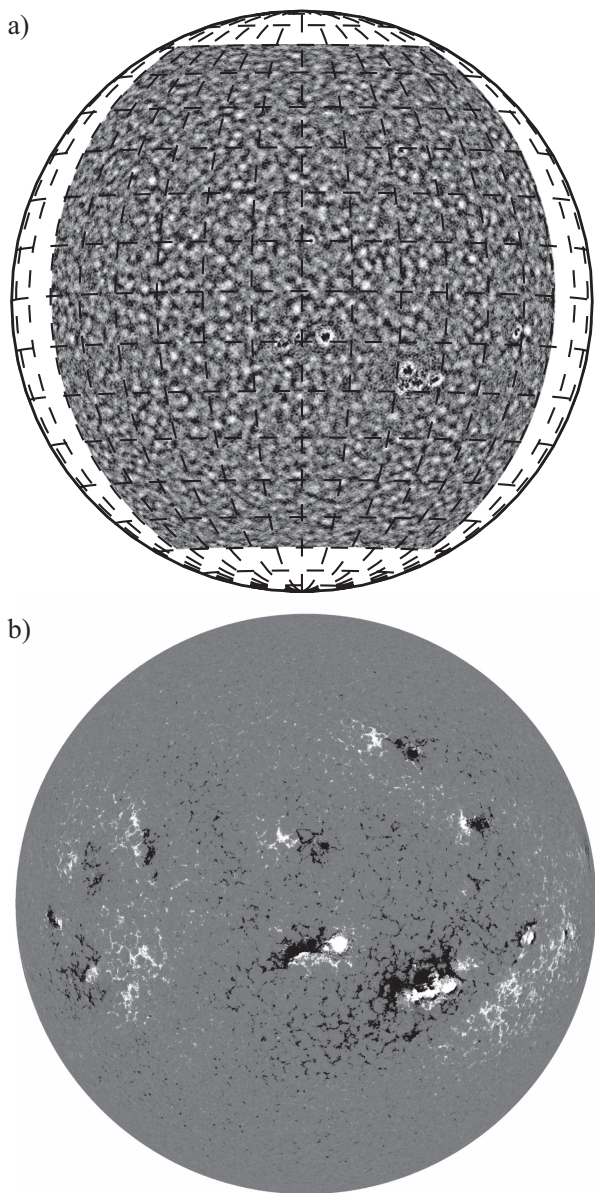
**Fig. 2.3** Comparison of the subsurface flow maps in the depth range from 1 to 3 Mm, obtained by using two different types of the travel measurements and two different approaches for calculation of the travel-time sensitivity functions: *red arrows* show the flow field obtained by using the Gabor-wavelet fitting technique and the raypath kernels (Kosovichev and Duvall 1997), the *blue arrows* are obtained by using the cross-correlation approach for the travel times (Gizon and Birch 2002), and the Born-approximation kernels (Birch and Kosovichev 2000). The *longest arrows* correspond to the velocity of about 1 km/s

around sunspots represents a complicated combination of converging flows towards the sunspot centers (displayed as dark dots in the divergence map) surrounded by outflows (represented as white rings). Such a pattern, similar to the flows shown in Figs. 2.3 and 2.5, has been previously studied using SOHO/MDI and Hinode data (Zhao et al. 2001, 2009, 2010). A new feature of the SDO/HMI analysis is that the HMI data allow us to reconstruct the flows in a shallow subsurface layer, and match these to the directly observed surface flows. This agreement provides more confidence in the helioseismic inferences.

Figure 2.5 shows a portion of the horizontal velocity map around an emerging active region NOAA 11726, during its development phase. This is the largest active region observed by the HMI instrument during the first 5 years of operation. The flow velocities are shown by arrows, and the photospheric magnetogram is represented by the color map. Such flow maps are obtained with 1-h sampling,



**Fig. 2.4** (a) A full-disk map showing the divergence of the horizontal velocity at the depth of 1–3 Mm, obtained on December 19, 2014, 12:00 UT. The *bright point-like areas* represent diverging supergranulation flows, the *dark areas* surrounded by *bright rings* represent flows converging beneath sunspots and diverging in the areas surrounding the sunspots. (b) The corresponding maps of the line-of-sight magnetic field obtained from the SDO Helioseismic and Magnetic Imager



although each map requires 8-h time series of Dopplergrams for the helioseismology analysis. The analysis of these maps indicates that the converging flows beneath the sunspots are developed simultaneously with the sunspot formation, as was previously found from analysis of the SOHO/MDI data (Kosovichev and Duvall 2006; Kosovichev 2009), and, probably, is closely associated with the mechanism of the sunspot formation. At the same time, large-scale diverging flows are developed



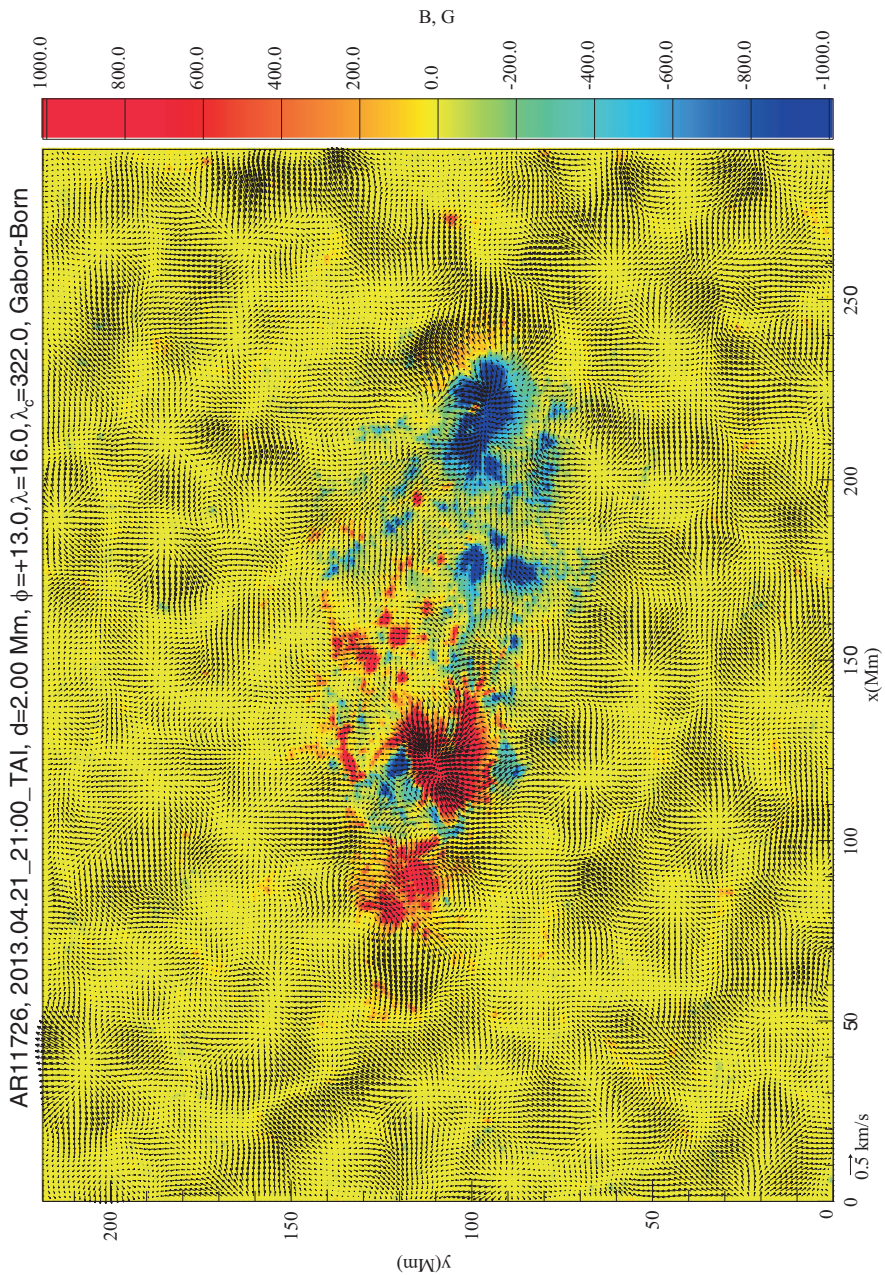


**Fig. 2.5** Arrows show the horizontal flow map in the active region NOAA 11726 at the depth of 2 Mm on April 21, 2013, 21:00 UT, about 2 days after its emergence from the interior. The *color background* image shows the surface magnetic field. The flow map is reconstructed by using the Gabor-wavelet technique for measuring the travel times, and the Born-approximation sensitivity kernels for the flow velocity inversion

around the active region, and are probably related to the well-known phenomenon of the surface ‘moat’ flow.

Outside the active region the flow pattern is mostly represented by supergranulation which, however, is clearly disturbed by the presence of the active region. It is interesting that the spatial averaging of these flow maps reveals a large-scale pattern of converging flows occupying a surrounding area which is significantly larger than the active region (Fig. 2.6). Such converging flows with the characteristic speed of about 50 m/s were first discovered by the ring-diagram technique (Haber et al. 2003). The origin of these flows is not understood, but our analysis shows that these flows are formed and stable only when the active region is fully developed, and, thus, they are not associated with the emergence of magnetic flux and formation of the active region.

The large-scale converging flows around active regions play an important role in the solar-cycle evolution of the meridional circulation (Haber et al. 2002; Zhao and Kosovichev 2004). The meridional circulation can be calculated from the reconstructed subsurface flow maps by averaging the North-South component of the flow velocity. Figure 2.7a shows a map of the North-South velocity component smoothed with a 5-deg Gaussian window.

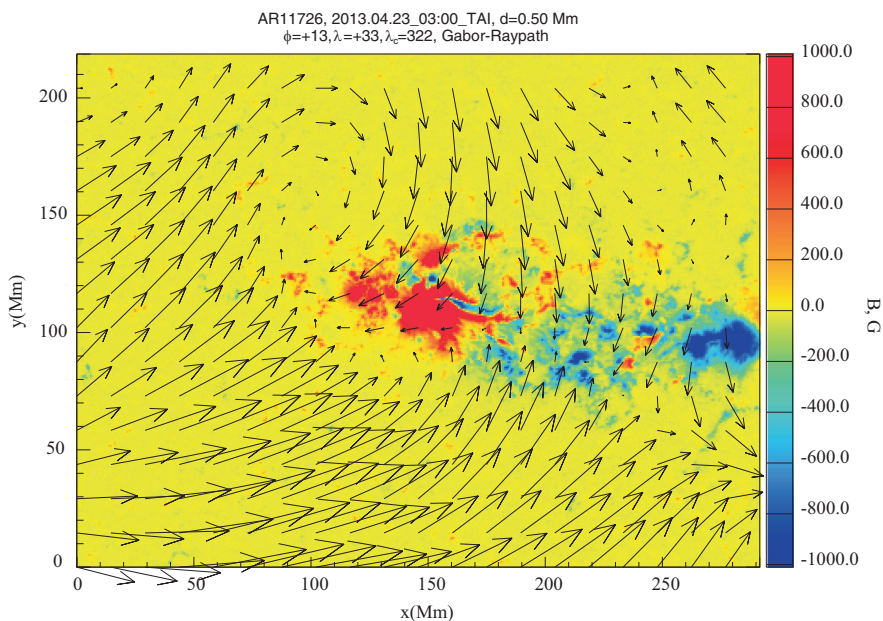


**Fig. 2.6** Arrows show the horizontal flow map around the active region NOAA 11726 at the depth of 0.3 Mm on April 23, 2013, 03:00 UT (when the active region is fully developed) after averaging the high-resolution flow map on a grid with a 15-degree sampling. The *color background image* shows the surface magnetic field. The typical flow speed is about 50 m/s

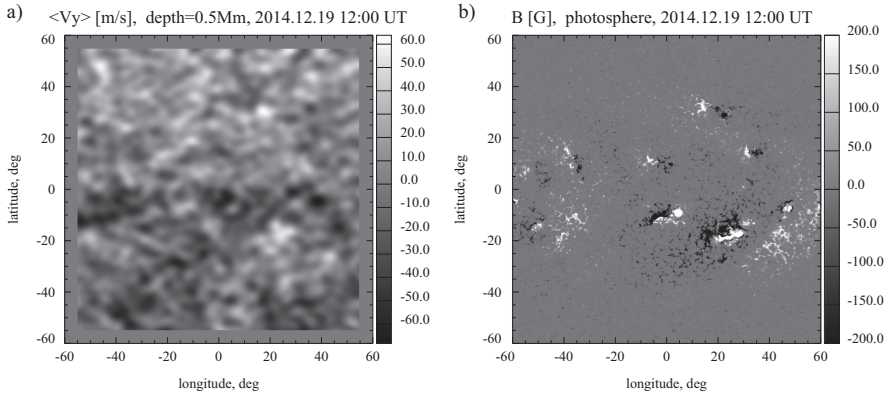


**Fig. 2.7** (a) A map of the North-South component of the subsurface flow velocity of December 12, 2014, 12:00 UT, smoothed with a 5 deg Gaussian window, reveals that the meridional flow pattern disturbed the converging flows around active regions. (b) The corresponding photospheric magnetogram map. *Red color* shows the positive polarity, the *blue color* shows the negative polarity

The appearance of the poleward trends in each hemisphere is apparent. It is interesting that the meridional circulation can be detected in a single flow map, but it is also important that the flow pattern correlates with the surface magnetic field map shown in Fig. 2.7b. The variations can be interpreted as caused by the large-scale converging flows around active regions. However, the strongest variations in this flow map seem to be in the areas of decaying active regions. Thus, it is important to investigate the formation and evolution of the converging flows during the whole evolution of active regions, from their formation to decay.

The evolution of meridional circulation is obtained by averaging the North-South velocity component over longitude and 1-month periods, and displaying the averages in the form of a time-latitude diagram (Fig. 2.8a). This diagram shows that the evolution of the subsurface meridional circulation correlates with the magnetic activity in each hemisphere. At the beginning of the current cycle most active regions emerged in the Northern hemisphere, where we see a strong variation of the meridional circulation speed: a sharp increase at low latitudes (in the 10–20 deg interval) and a decrease at mid latitudes (in the 20–30 deg range). A similar variation in the Southern hemisphere is observed in 2014–2015 when most magnetic activity was in the South (Fig. 2.9b).

Such variations of the meridional circulation may affect the magnetic flux transport and the polar magnetic field polarity reversal. However, this link has not been fully established (Švanda et al. 2007a,b, 2008). Figure 2.8b shows the variation of the mean (averaged over the whole period) meridional circulation profile with depth. It appears that at a depth of  $\sim 10$  Mm the latitudinal variations are significantly reduced, and at the depth of  $\sim 20$  Mm almost entirely disappear. Therefore, if the large-scale magnetic flux is anchored at this depth or lower then its transport is not affected by the meridional flow variations.



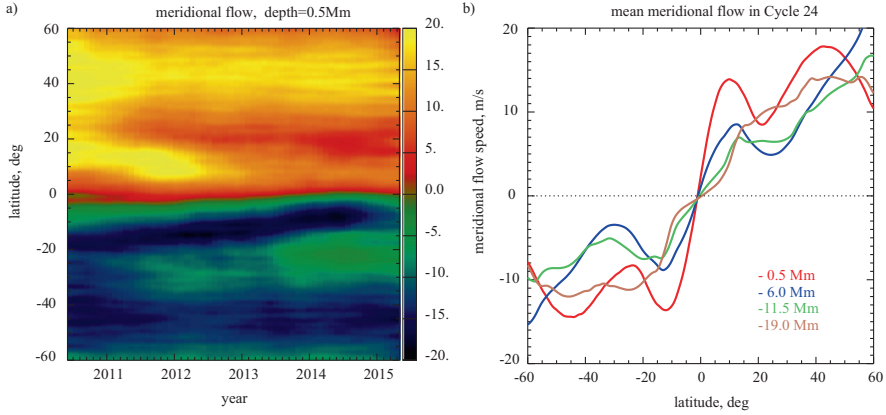


**Fig. 2.8** (a) Evolution of the subsurface meridional flows obtained from the 5-years of the SDO/HMI observations during Solar Cycle 24. The *red* and *yellow* colors show the flow components towards the North pole, the *green* and *blue* colors show the South-ward flow. The color scale range is from  $-20$  to  $20$  m/s. (b) The mean meridional flow averaged for the whole period of observations at four different depths

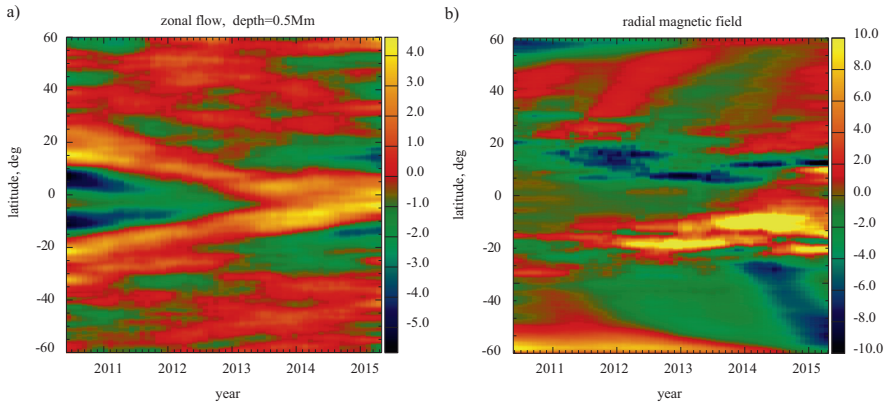


**Fig. 2.9** (a) The evolution of the subsurface zonal flows ('torsional oscillation') during the first 5 years of the SDO observations, covering the raising phase of Solar Cycle 24. The flow map (in m/s) is obtained by averaging of the azimuthal flow component of longitude and 1-month time, subtracting the mean rotational velocity from each of the 1-month averaged profile, and then stacking the residual velocity profiles and smoothing with 1-year running window to remove the annual variations due to the inclination of the Earth orbit. The *yellow* and *red* colors correspond to the zonal flows faster than the mean solar rotation at the same depth, and the *blue* color shows the slower rotating regions. (b) The corresponding magnetic 'butterfly' diagram from the SDO/HMI data, showing the evolution of the mean radial magnetic field (in G) in the solar photosphere during the same period

Solar-cycle variations of the differential rotation are also of great interest for the understanding of the mechanisms of solar activity. These variations, known as ‘torsional oscillation’, have been detected from the surface Doppler-shift maps (Howard and Labonte 1980; Ulrich 2001), and by global (Kosovichev and Schou 1997) and local (Zhao and Kosovichev 2004) helioseismology. The high-resolution flow maps from SDO/HMI provide new opportunities for investigating the detailed structure and evolution of these flows. Figure 2.9a shows the time-latitude diagram of variations of the differential rotation during the 5 years of the SDO/HMI observations. These variations are relative to the mean differential rotation profile averaged for the whole period, and smoothed with a 1-year window to remove the orbital variations. As it was established before, the zonal flow closely correlates with the magnetic butterfly diagram (Fig. 2.9b). However, our results also show the North-South asymmetry of the flows, which follows the asymmetry of the magnetic activity.

The flow maps allow us to investigate other important properties of the subsurface dynamics of the Sun, which previously were not accessible. For illustration, in Fig. 2.10a we show a map of the kinetic helicity proxy calculated as  $\nabla \mathbf{v}_h \cdot (\nabla \times \mathbf{v}_h)_z$ , where  $\mathbf{v}_h$  is the horizontal velocity component. By looking at this map one can notice that the Northern hemisphere is darker than the Southern hemisphere, and that the asymmetry is particularly pronounced in the supergranulation cells. After the longitudinal and time averaging of the individual helicity proxy maps we obtain the time-latitude diagram (Fig. 2.10b), which shows that the kinetic helicity does not vary on this time scale. This result puts constraints on the dynamo theories, and also shows that the supergranulation flows are likely a primary source of the near-surface helicity.

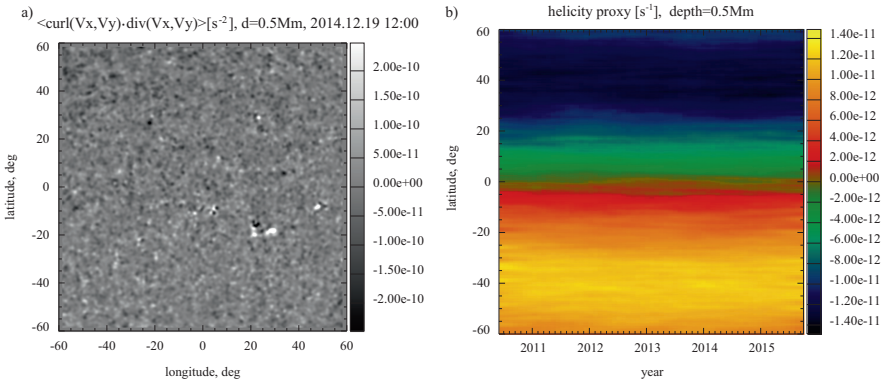


**Fig. 2.10** (a) The proxy of kinetic helicity density,  $\nabla \mathbf{v}_h \cdot (\nabla \times \mathbf{v}_h)_z$ , calculated from the flow map of December 12, 2014, 12:00 UT, reveals a systematic North-South asymmetry in local sources associated with supergranulation. (b) The evolution of the mean helicity proxy during the observed period of Solar Cycle 24

## 2.4 Conclusion

The initial analysis of the subsurface flow maps reconstructed from the 5 years of SDO/HMI data by time-distance helioseismology reveals the great potential for studying and understanding the dynamics of the quiet-Sun and active regions, and the evolution with the solar cycle. In particular, our results show that the emergence and evolution of active regions are accompanied by multi-scale flow patterns. Beneath the sunspot, during their formation, we observe appearance of flows converging towards the sunspot center, and also the ‘moat’-like flows diverging from the active region in the surrounding regions. On the larger scale, revealed by averaging the high-resolution flow maps, we find a pattern of flows converging towards the active region. This pattern is formed when the active region is fully developed. On the global-Sun scale, the flow maps allow us to investigate the structure and evolution of the meridional flows. In particular, we find that the meridional flows display the North-South asymmetry closely correlating with the magnetic activity. The latitudinal variations of the meridional circulation speed, which are probably related to the large-scale converging flows, are mostly confined in a shallow subsurface layers. Therefore, these variations do not necessarily affect the magnetic flux transport. The North-South asymmetry is also pronounced in the variations of the differential rotation (‘torsional oscillation’). The calculations of a proxy of the subsurface kinetic helicity density show that the helicity does not vary during the solar cycle, and that the supergranulation is a likely source of the near-surface helicity. These initial results are obtained from the analysis of a small sample of flow maps produced by the SDO/HMI time-distance helioseismology pipeline. Further detailed investigations are required for understanding the complicated subsurface dynamics of the Sun.

**Acknowledgements** This work was supported by the CNRS, and NASA grants NNX09AJ85G and NNX14AB70G.

## References

- Birch, A. C., & Gizon, L. (2007). Linear sensitivity of helioseismic travel times to local flows. *Astronomische Nachrichten*, 328, 228. doi:10.1002/asna.200610724. 1002.2338.
- Birch, A. C., & Kosovichev, A. G. (2000). Travel time sensitivity kernels. *Solar Physics*, 192, 193–201. doi:10.1023/A:1005283526062. <http://www.adsabs.harvard.edu/abs/2000SoPh..192..193B>.
- Birch, A. C., & Kosovichev, A. G. (2001). The born approximation in time-distance helioseismology. In A. Wilson & P. L. Pallé (Eds.), *SOHO 10/GONG 2000 Workshop: Helio- and Asteroseismology at the Dawn of the Millennium* (Vol. 464, pp. 187–190). ESA Special Publication. <http://www.adsabs.harvard.edu/abs/2001ESASP464..187B>.
- Birch, A. C., Kosovichev, A. G., Price, G. H., & Schlottmann, R. B. (2001). The accuracy of the born and ray approximations in time-distance helioseismology. *The Astrophysical Journal*, 561, L229–L232. doi:10.1086/324766. <http://www.adsabs.harvard.edu/abs/2001ApJ...561L.229B>.



- Birch, A. C., Kosovichev, A. G., & Duvall, T. L., Jr. (2004). Sensitivity of acoustic wave travel times to sound-speed perturbations in the solar interior. *The Astrophysical Journal*, 608, 580–600. doi:10.1086/386361. <http://www.adsabs.harvard.edu/abs/2004ApJ...608..580B>.
- Birch, A. C., Parchevsky, K. V., Braun, D. C., & Kosovichev, A. G. (2011). “Hare and hounds” tests of helioseismic holography. *Solar Physics*, 272, 11–28. doi:10.1007/s11207-011-9799-1. <http://www.adsabs.harvard.edu/abs/2011SoPh..272...11B>.
- Couvidat, S., Zhao, J., Birch, A. C., Kosovichev, A. G., Duvall, T. L., Parchevsky, K., et al. (2012). Implementation and comparison of acoustic travel-time measurement procedures for the Solar Dynamics Observatory/HelioSeismic and Magnetic Imager time – distance helioseismology pipeline. *Solar Physics*, 275, 357–374. doi:10.1007/s11207-010-9652-y. <http://www.adsabs.harvard.edu/abs/2012SoPh..275..357C>.
- Duvall, T. L., Jr., Jefferies, S. M., Harvey, J. W., & Pomerantz, M. A. (1993). Time-distance helioseismology. *Nature*, 362, 430–432. doi:10.1038/362430a0.
- Gizon, L., & Birch, A. C. (2002). Time-distance helioseismology: The forward problem for random distributed sources. *The Astrophysical Journal*, 571, 966–986. doi:10.1086/340015.
- Godier, S., & Rozelot, J. P. (2001). A new outlook on the ‘differential theory’ of the solar quadrupole moment and oblateness. *Solar Physics*, 199, 217–229. doi:10.1023/A:1010354901960. <http://www.adsabs.harvard.edu/abs/2001SoPh..199..217G>.
- Gough, D. O., & Toomre, J. (1983). On the detection of subphotospheric convective velocities and temperature fluctuations. *Solar Physics*, 82, 401–410. doi:10.1007/BF00145579.
- Haber, D. A., Hindman, B. W., Toomre, J., Bogart, R. S., Larsen, R. M., & Hill, F. (2002). Evolving submerged meridional circulation cells within the upper convection zone revealed by ring-diagram analysis. *The Astrophysical Journal*, 570, 855–864. doi:10.1086/339631.
- Haber, D. A., Hindman, B. W., & Toomre, J. (2003). Interaction of solar subsurface flows with major active regions. In H. Sawaya-Lacoste (Ed.), *GONG+ 2002. Local and global helioseismology: The present and future* (Vol. 517, pp. 103–108). ESA Special Publication
- Hartlep, T., Zhao, J., Kosovichev, A. G., & Mansour, N. N. (2013). Solar wave-field simulation for testing prospects of helioseismic measurements of deep meridional flows. *The Astrophysical Journal*, 762, 132. doi:10.1088/0004-637X/762/2/132. <http://www.adsabs.harvard.edu/abs/2013ApJ...762..132H>. 1209.4602.
- Howard, R., & Labonte, B. J. (1980). The Sun is observed to be a torsional oscillator with a period of 11 years. *The Astrophysical Journal*, 239, L33–L36. doi:10.1086/183286.
- Jacobsen, B., Møller, I., Jensen, J., & Efferso, F. (1999). Multichannel deconvolution, mcd, in geophysics and helioseismology. *Physics and Chemistry of the Earth A*, 24, 215–220. doi:10.1016/S1464-1895(99)00021-6.
- Kitiashvili, I. N., Kosovichev, A. G., Mansour, N. N., & Wray, A. A. (2011). Excitation of acoustic waves by vortices in the quiet Sun. *The Astrophysical Journal*, 727, L50. doi:10.1088/2041-8205/727/2/L50. <http://www.adsabs.harvard.edu/abs/2011ApJ...727L..50K>. 1011.3775.
- Kosovichev, A. G. (1996a). Tomographic imaging of the Sun’s interior. *The Astrophysical Journal*, 461, L55. doi:10.1086/309989. <http://www.adsabs.harvard.edu/abs/1996ApJ...461L..55K>.
- Kosovichev, A. G. (1996b). Helioseismic constraints on the gradient of angular velocity at the base of the solar convection zone. *The Astrophysical Journal*, 469, L61. doi:10.1086/310253. <http://www.adsabs.harvard.edu/abs/1996ApJ...469L..61K>.
- Kosovichev, A. G. (2009). Photospheric and subphotospheric dynamics of emerging magnetic flux. *Space Science Reviews*, 144, 175–195. doi:10.1007/s11214-009-9487-8. <http://www.adsabs.harvard.edu/abs/2009SSRv..144..175K>. 0901.0035.
- Kosovichev, A. G. (2012). Local helioseismology of sunspots: Current status and perspectives. *Solar Physics*, 279, 323–348. doi:10.1007/s11207-012-9996-6. <http://www.adsabs.harvard.edu/abs/2012SoPh..279..323K>.
- Kosovichev, A. G., & Duvall, T. L. (2006). Active region dynamics. *Space Science Reviews*, 124, 1–12. doi:10.1007/s11214-006-9112-z. <http://www.adsabs.harvard.edu/abs/2006SSRv..124....1K>.
- Kosovichev, A. G., & Duvall, T. L., Jr. (1997). Acoustic tomography of solar convective flows and structures. In F. P. Pijpers, J. Christensen-Dalsgaard, & C. S. Rosenthal (Eds.),

- SCORe'96: Solar Convection and Oscillations and Their Relationship* (Vol. 225, pp. 241–260). Astrophysics and Space Science Library. <http://www.adsabs.harvard.edu/abs/1997ASSL..225..241K>.
- Kosovichev, A. G., & Schou, J. (1997). Detection of zonal shear flows beneath the Sun's surface from f-mode frequency splitting. *The Astrophysical Journal*, 482, L207–L210. doi:10.1086/310708. <http://www.adsabs.harvard.edu/abs/1997ApJ...482L.207K>.
- Kosovichev, A. G., Duvall, T. L., Jr., & Scherrer, P. H. (2000). Time-distance inversion methods and results – (invited review). *Solar Physics*, 192, 159–176. doi:10.1023/A:1005251208431. <http://www.adsabs.harvard.edu/abs/2000SoPh..192..159K>.
- Kosovichev, A. G., Basu, S., Bogart, R., Duvall, T. L., Jr., Gonzalez-Hernandez, I., Haber, D., et al. (2011). Local helioseismology of sunspot regions: Comparison of ring-diagram and time-distance results. *Journal of Physics Conference Series*, 271(1), 012005. doi:10.1088/1742-6596/271/1/012005. <http://www.adsabs.harvard.edu/abs/2011JPhCS.271a2005K>. 1011.0799.
- Lindsey, C., & Braun, D. C. (2000). Basic principles of solar acoustic holography – (invited review). *Solar Physics*, 192, 261–284. doi:10.1023/A:1005227200911.
- Liu, Y., Zhao, J., & Schuck, P. W. (2013). Horizontal flows in the photosphere and subphotosphere of two active regions. *Solar Physics*, 287, 279–291. doi:10.1007/s11207-012-0089-3.
- Parchevsky, K. V., & Kosovichev, A. G. (2009). Numerical simulation of excitation and propagation of helioseismic MHD waves: Effects of inclined magnetic field. *The Astrophysical Journal*, 694, 573–581. doi:10.1088/0004-637X/694/1/573. <http://www.adsabs.harvard.edu/abs/2009ApJ...694..573P>. 0806.2897.
- Parchevsky, K. V., Zhao, J., Hartlep, T., & Kosovichev, A. G. (2014). Verification of the helioseismology travel-time measurement technique and the inversion procedure for sound speed using artificial data. *The Astrophysical Journal*, 785, 40. doi:10.1088/0004-637X/785/1/40. <http://www.adsabs.harvard.edu/abs/2014ApJ...785...40P>.
- Pipin, V. V., & Kosovichev, A. G. (2011). The subsurface-shear-shaped solar  $\alpha\Omega$  dynamo. *The Astrophysical Journal*, 727, L45. doi:10.1088/2041-8205/727/2/L45. <http://www.adsabs.harvard.edu/abs/2011ApJ...727L..45P>. 1011.4276.
- Reiter, J., Rhodes, E. J., Jr., Kosovichev, A. G., Schou, J., Scherrer, P. H., & Larson, T. P. (2015). A method for the estimation of p-mode parameters from averaged solar oscillation power spectra. *The Astrophysical Journal*, 803, 92. doi:10.1088/0004-637X/803/2/92. <http://www.adsabs.harvard.edu/abs/2015ApJ...803...92R>. 1504.07493.
- Scherrer, P. H., Schou, J., Bush, R. I., Kosovichev, A. G., Bogart, R. S., Hoeksema, J. T., et al. (2012). The Helioseismic and Magnetic Imager (HMI) investigation for the Solar Dynamics Observatory (SDO). *Solar Physics*, 275, 207–227. doi:10.1007/s11207-011-9834-2. <http://www.adsabs.harvard.edu/abs/2012SoPh..275..207S>.
- Schou, J., Antia, H. M., Basu, S., Bogart, R. S., Bush, R. I., Chitre, S. M., et al. (1998). Helioseismic studies of differential rotation in the solar envelope by the solar oscillations investigation using the Michelson Doppler Imager. *The Astrophysical Journal*, 505, 390–417. doi:10.1086/306146. <http://www.adsabs.harvard.edu/abs/1998ApJ...505..390S>.
- Ulrich, R. K. (2001). Very long lived wave patterns detected in the solar surface velocity signal. *The Astrophysical Journal*, 560, 466–475. doi:10.1086/322524.
- Švanda, M., Kosovichev, A. G., & Zhao, J. (2007a). Speed of meridional flows and magnetic flux transport on the Sun. *The Astrophysical Journal*, 670, L69–L72. doi:10.1086/524059. <http://www.adsabs.harvard.edu/abs/2007ApJ...670L..69S>. 0710.0590.
- Švanda, M., Zhao, J., & Kosovichev, A. G. (2007b). Comparison of large-scale flows on the Sun measured by time-distance helioseismology and local correlation tracking. *Solar Physics*, 241, 27–37. doi:10.1007/s11207-007-0333-4. <http://www.adsabs.harvard.edu/abs/2007SoPh..241...27S>. astro-ph/0701171.
- Švanda, M., Kosovichev, A. G., & Zhao, J. (2008). Effects of solar active regions on meridional flows. *The Astrophysical Journal*, 680, L161–L164. doi:10.1086/589997. <http://www.adsabs.harvard.edu/abs/2008ApJ...680L.161S>. 0805.1789.

- Zhao, J., & Kosovichev, A. G. (2004). Torsional oscillation, meridional flows, and vorticity inferred in the upper convection zone of the Sun by time-distance helioseismology. *The Astrophysical Journal*, 603, 776–784. doi:10.1086/381489. <http://www.adsabs.harvard.edu/abs/2004ApJ...603..776Z>.
- Zhao, J., Kosovichev, A. G., & Duvall T. L., Jr. (2001). Investigation of mass flows beneath a sunspot by time-distance helioseismology. *The Astrophysical Journal*, 557, 384–388. doi:10.1086/321491. <http://www.adsabs.harvard.edu/abs/2001ApJ...557..384Z>.
- Zhao, J., Kosovichev, A. G., & Sekii, T. (2009). Subsurface structures and flow fields of an active region observed by Hinode. In B. Lites, M. Cheung, T. Magara, J. Mariska, & K. Reeves (Eds.), *The Second Hinode Science Meeting: Beyond Discovery-Toward Understanding*. Astronomical Society of the Pacific Conference Series (Vol. 415, p. 411). <http://www.adsabs.harvard.edu/abs/2009ASPC..415..411Z>.
- Zhao, J., Kosovichev, A. G., & Sekii, T. (2010). High-resolution helioseismic imaging of subsurface structures and flows of a solar active region observed by Hinode. *The Astrophysical Journal*, 708, 304–313. doi:10.1088/0004-637X/708/1/304. <http://www.adsabs.harvard.edu/abs/2010ApJ...708..304Z>. 0911.1161.
- Zhao, J., Couvidat, S., Bogart, R. S., Parchevsky, K. V., Birch, A. C., Duvall, T. L., et al. (2012) Time-distance helioseismology data-analysis pipeline for Helioseismic and Magnetic Imager onboard Solar Dynamics Observatory (SDO/HMI) and its initial results. *Solar Physics*, 275, 375–390. doi:10.1007/s11207-011-9757-y. <http://www.adsabs.harvard.edu/abs/2012SoPh..275..375Z>. 1103.4646.

Cartography of the Sun and the Stars

Rozelot, J.-P.; Neiner, C. (Eds.)

2016, X, 206 p. 78 illus., 48 illus. in color., Softcover

ISBN: 978-3-319-24149-4